

NNLO corrections to $\bar{B} \rightarrow X_u \ell \bar{\nu}_\ell$ and the determination of $|V_{ub}|$

C. GREUB^(a), M. NEUBERT^(b), AND B. D. PECJAK^(b)

^(a)*Albert Einstein Center for Fundamental Physics, Institute for Theoretical Physics,
Univ. of Bern, CH-3012 Bern, Switzerland*

^(b)*Johannes Gutenberg-Universität, D-55099 Mainz, Germany*

Abstract

We study the impact of next-to-next-to-leading order (NNLO) QCD corrections on partial decay rates in $\bar{B} \rightarrow X_u \ell \bar{\nu}_\ell$ decays, at leading-order in the $1/m_b$ expansion for shape-function kinematics. These corrections are implemented within a modified form of the BLNP framework, which allows for arbitrary variations of the jet scale $\mu_i \sim 1.5$ GeV. Our analysis includes a detailed comparison between resummed and fixed-order perturbation theory, and between the complete NNLO results and those obtained in the large- β_0 approximation. For the default choice $\mu_i = 1.5$ GeV used in current extractions of $|V_{ub}|$ within the BLNP framework, the NNLO corrections induce significant downward shifts in the central values of partial decay rates with cuts on the hadronic variable P_+ , the hadronic invariant mass, and the lepton energy. At the same time, perturbative uncertainties are reduced, especially those at the jet scale, which are the dominant ones at next-to-leading order (NLO). For higher values of μ_i and in fixed-order perturbation theory, the shifts between NLO and NNLO are more moderate. We combine our new results with known power-suppressed terms in order to illustrate the implications of our analysis on the determination of $|V_{ub}|$ from inclusive decays.

1 Introduction

The CKM element $|V_{ub}|$ is a fundamental parameter of flavor physics. It measures the strength of $b \rightarrow u$ quark transitions and determines the length of the side of the unitarity triangle opposite to the angle β . The combined work of many theorists and experimentalists has allowed to determine this parameter from data on both inclusive and exclusive semi-leptonic $b \rightarrow u$ decays; a summary of current results can be found in, for instance, [1–3]. A characteristic feature of these analyses is that the value of $|V_{ub}|$ deduced from inclusive decays is consistently higher than that from exclusive decays. The need to resolve this discrepancy motivates systematic improvements on all fronts.

The goal of this paper is to improve the theory predictions for the inclusive decays $\bar{B} \rightarrow X_u \ell \bar{\nu}_\ell$ by including recently calculated next-to-next-to-leading order (NNLO) perturbative corrections to the partial decay rates used in the extraction of $|V_{ub}|$. In general, these partial rates are available only in the portion of phase space referred to as the shape-function region, where the hadronic final state is a jet carrying an energy of order m_b and an invariant mass squared of order $m_b \Lambda_{\text{QCD}}$. A local operator product expansion is not valid in this region, and results are obtained through a factorization formalism, as a convolution of perturbative hard-scattering kernels with non-perturbative shape functions [4–6]. Different approaches to this factorization have been put forth in the literature, going under the names of BLNP [7, 8], GGOU [9], and the dressed-gluon exponentiation [10].

In this paper we implement the NNLO perturbative corrections within the BLNP framework. In this approach, techniques from soft-collinear effective theory (SCET) [11–13] are used to obtain an arbitrary partial decay rate as an expansion in $1/m_b$, according to

$$\Gamma_u = \Gamma_u^{(0)} + [\Gamma_u^{(1)} + \Gamma_u^{(2)} + \dots]. \quad (1)$$

The first term is of leading order in the heavy-quark expansion, whereas the terms in the square brackets account for power-suppressed effects and are estimated up to order $1/m_b^2$. The NNLO corrections studied in the current paper affect only the leading-order term $\Gamma_u^{(0)}$. For kinematic cuts limited to the shape-function region, this term obeys a factorization formula of the schematic form [7, 14–16]

$$\Gamma_u^{(0)} \sim [H \cdot J](\mu_f) \otimes S(\mu_f), \quad (2)$$

where the symbol \otimes denotes a convolution. The factorization formula contains a hard function H , related to physics at the hard scale $\mu_h \sim m_b$, a jet function J , related to physics at the intermediate scale $\mu_i \sim (m_b \Lambda_{\text{QCD}})^{1/2} \sim 1.5 \text{ GeV}$, and a non-perturbative shape function S , describing the internal soft dynamics of the B meson. A thorough analysis of this leading-power term at next-to-leading order (NLO) in renormalization-group (RG) improved perturbation theory was performed in [8]. We can extend this analysis to NNLO by putting together a number of pieces, which we describe in Section 2. In addition to calculating the higher-order perturbative corrections, we also modify the BLNP framework to allow for variations of the arbitrary matching scale μ_i at which the jet function is calculated. This allows us to study the perturbative uncertainties associated with this scale, and makes for a straightforward matching with fixed-order perturbation theory, where logarithms between the hard and intermediate scales are not resummed. In the numerical analysis in Section 3 we apply our new results to partial decay rates with cuts on the hadronic variable P_+ , the hadronic invariant mass, and the lepton energy.

Our main findings are that the dependence on the scale μ_i is sizeable at NLO and still significant even at NNLO, and that for the default choice $\mu_i = 1.5$ GeV typically used in the BNLFP framework the NNLO corrections tend to shift the partial decay rates downward by a significant amount. We also study some qualitative aspects of the perturbative series by comparing results obtained in resummed and fixed-order perturbation theory, and with those obtained in the large- β_0 approximation. To illustrate the significance of our results for the extraction of $|V_{ub}|$, in Section 4 we combine the NNLO corrections to the leading-order term with known power corrections and experimental data in order to extract sample values of $|V_{ub}|$ for several partial rates. For the particular choice of intermediate scale $\mu_i = 2.0$ GeV, the effect of the NNLO corrections is to raise the central value of $|V_{ub}|$ by slightly less than 10% compared to the results at NLO; for higher choices of the intermediate scale and in fixed-order perturbation theory, the corrections are more moderate. We summarize our findings in Section 5.

2 Partial decay rates in SCET

In this section we briefly review the BLNP formalism as applied to inclusive semi-leptonic $b \rightarrow u$ decays. We begin by recalling the master formula for an arbitrary partial decay rate derived in [8], expressed in terms of the hadronic variables

$$P_- = E_X + |\vec{P}_X|, \quad P_+ = E_X - |\vec{P}_X|. \quad (3)$$

It is given by

$$\frac{d\Gamma_u(y_{\max}, y_0)}{dP_+} = \begin{cases} \Gamma_u^A(y_{\max}) & ; \quad y_{\max} \leq y_0, \\ \Gamma_u^A(y_0) + \Gamma_u^B & ; \quad y_{\max} > y_0, \end{cases} \quad (4)$$

where

$$\begin{aligned} \Gamma_u^A(y_i) &= \frac{G_F^2 |V_{ub}|^2}{96\pi^3} (M_B - P_+)^5 \int_0^{y_i} dy y^2 [(3 - 2y) f_1 + 6(1 - y) f_2 + y f_3], \\ \Gamma_u^B &= \frac{G_F^2 |V_{ub}|^2}{96\pi^3} (M_B - P_+)^5 \int_{y_0}^{y_{\max}} dy y_0 \\ &\quad \times [(6y(1 + y_0) - 6y^2 - y_0(3 + 2y_0)) f_1 + 6y(1 - y) f_2 + y_0(3y - 2y_0) f_3]. \end{aligned} \quad (5)$$

The dimensionless variables y , y_0 , and y_{\max} are defined as

$$y = \frac{P_- - P_+}{M_B - P_+}, \quad y_{\max} = \frac{P_-^{\max} - P_+}{M_B - P_+}, \quad y_0 = \frac{P_l^{\max} - P_+}{M_B - P_+} = 1 - \frac{2E_0}{M_B - P_+}, \quad (6)$$

and we have introduced the quantity E_0 , which is the minimum allowed lepton energy. The values of y_{\max} and the integration range for P_+ depend on the specifics of the partial decay rate under consideration. For cuts $P_+ < \Delta_P$ and on the lepton energy, we have $y_{\max} = 1$ and $0 < P_+ < \min(\Delta_P, M_B - 2E_0)$. For a cut on the hadronic invariant mass, $M_X < M_0$, we have

$$y_{\max} = \frac{\min(M_B, M_0^2/P_+) - P_+}{M_B - P_+} \quad (7)$$

and $0 < P_+ < M_0$.

The scalar functions f_i are obtained as an expansion in $1/m_b$. The leading-order term has the form (2) and reads

$$f_i^{(0)}(P_+, y) = H_{ui}(y, m_b, \mu_f) \int_0^{P_+} d\hat{\omega} y m_b J(y m_b (P_+ - \hat{\omega}), \mu_f) \hat{S}(\hat{\omega}, \mu_f). \quad (8)$$

As written, (8) achieves a factorization of perturbative and non-perturbative physics. The hard functions H_{ui} contain physics at the scale m_b , the jet function J contains physics at the jet scale $(m_b \Lambda_{\text{QCD}})^{1/2}$, and the shape-function S is a non-perturbative matrix element in heavy-quark effective theory (HQET) [4, 6]. In SCET, one usually assumes the parametric limit where the hard scale is much larger than the jet scale, in which case any choice of μ_f leads to large perturbative logarithms in either H or J . To solve this problem one first calculates these functions at matching scales where they contain no large logarithms, and then evolves them to a common scale μ_f using the renormalization group (RG). Also, within the effective-theory framework, it is natural to extract the non-perturbative shape function at a low scale μ_0 , and then evolve it to the scale μ_f . The RG evolution can be achieved using results from [7, 17] for the hard and shape functions, and [18] for the jet function. For convenience, we list the solutions here:

$$H_{ui}(y, m_b, \mu_f) = y^{-2a_\Gamma(\mu_h, \mu_f)} \exp \left[2S(\mu_h, \mu_f) - 2a_\Gamma(\mu_h, \mu_f) \ln \frac{m_b}{\mu_h} - 2a_{\gamma'}(\mu_h, \mu_f) \right] \times H_{ui}(y, m_b, \mu_h), \quad (9)$$

$$J(p^2, \mu_f) = \exp \left[-4S(\mu_i, \mu_f) + 2a_{\gamma J}(\mu_i, \mu_f) \right] \tilde{j}(\partial_{\eta_J}, \mu_i) \left[\frac{1}{p^2} \left(\frac{p^2}{\mu_i^2} \right)^{\eta_J} \right]_* \frac{e^{-\gamma_E \eta_J}}{\Gamma(\eta_J)},$$

$$\hat{S}(\hat{\omega}, \mu_f) = \exp \left[2S(\mu_0, \mu_f) + 2a_{\gamma' - \gamma J}(\mu_0, \mu_f) \right] \frac{e^{-\gamma_E \eta_S}}{\Gamma(\eta_S)} \int_0^{\hat{\omega}} d\hat{\omega}' \frac{\hat{S}(\hat{\omega}', \mu_0)}{\mu_0^{\eta_S} (\hat{\omega} - \hat{\omega}')^{1-\eta_S}}.$$

The RG exponents read [7]

$$S(\nu, \mu) = - \int_{\alpha_s(\nu)}^{\alpha_s(\mu)} d\alpha \frac{\Gamma_{\text{cusp}}(\alpha)}{\beta(\alpha)} \int_{\alpha_s(\nu)}^{\alpha} \frac{d\alpha'}{\beta(\alpha')}, \quad a_\Gamma(\nu, \mu) = - \int_{\alpha_s(\nu)}^{\alpha_s(\mu)} d\alpha \frac{\Gamma_{\text{cusp}}(\alpha)}{\beta(\alpha)}, \quad (10)$$

and similarly for $a_{\gamma'}$ ($a_{\gamma J}$), but with Γ_{cusp} replaced by the anomalous dimensions of the hard (jet) function. We have defined $\eta_J = 2a_\Gamma(\mu_i, \mu_f)$, $\eta_S = 2a_\Gamma(\mu_f, \mu_0)$, and \tilde{j} is the Laplace transform of J . Finally, the star distribution is defined as

$$\int_0^{Q^2} dp^2 \left[\frac{1}{p^2} \left(\frac{p^2}{\mu^2} \right)^\eta \right]_* f(p^2) = \int_0^{Q^2} dp^2 \frac{f(p^2) - f(0)}{p^2} \left(\frac{p^2}{\mu^2} \right)^\eta + \frac{f(0)}{\eta} \left(\frac{Q^2}{\mu^2} \right)^\eta. \quad (11)$$

Inserting the above results into the factorization formula (8), and using the general relations [19]

$$a_\Gamma(\mu_1, \mu_2) + a_\Gamma(\mu_2, \mu_3) = a_\Gamma(\mu_1, \mu_3),$$

$$S(\mu_1, \mu_2) + S(\mu_2, \mu_3) = S(\mu_1, \mu_3) + \ln \frac{\mu_1}{\mu_2} a_\Gamma(\mu_2, \mu_3), \quad (12)$$

one is left with

$$\begin{aligned}
f_i^{(0)}(P_+, y) = \exp & \left[2S(\mu_h, \mu_i) - 2S(\mu_i, \mu_0) + 2a_{\gamma^J}(\mu_i, \mu_0) - 2a_{\gamma'}(\mu_h, \mu_0) \right. \\
& \left. - 2a_\Gamma(\mu_h, \mu_i) \ln \frac{m_b}{\mu_h} \right] \times H_{ui}(y, m_b, \mu_h) y^{-2a_\Gamma(\mu_h, \mu_i)} \\
& \times \tilde{j} \left(\ln \frac{m_b y}{\mu_i} + \partial_\eta, \mu_i \right) \frac{e^{-\gamma_E \eta}}{\Gamma(\eta)} \int_0^{P_+} d\hat{\omega} \left[\frac{1}{P_+ - \hat{\omega}} \left(\frac{P_+ - \hat{\omega}}{\mu_i} \right)^\eta \right]_* \hat{S}(\hat{\omega}, \mu_0),
\end{aligned} \tag{13}$$

where now $\eta = 2a_\Gamma(\mu_i, \mu_0)$. Note that the dependence on the arbitrary factorization scale μ_f has disappeared.

Equations (4) and (13) are the master formulas for calculating the leading-power contribution to a given partial decay rate in RG-improved perturbation theory. The results are formally independent of the matching scales μ_h and μ_i , but a residual dependence remains when truncating the perturbative expansion at a given order. Moreover, by setting $\mu_h = \mu_i = \mu$, one recovers fixed-order perturbation theory directly from the resummed results. The product of matching functions $(H \cdot J)(\mu)$ is combined into a single coefficient function $C(\mu)$, and the RG exponents serve to evolve the shape-function from the scale μ_0 to μ . We shall discuss and compare the perturbative uncertainties in both resummed and fixed-order perturbation theory at LO, NLO, and NNLO in the following section. The scale μ_0 plays a special role in the analysis. We shall choose this as the scale at which we model the non-perturbative shape function; more details will be given below.

We can evaluate the master formula (13) at NNLO in RG-improved perturbation theory by gathering together a number of results available in the literature. By NNLO, we mean the approximation which captures all of the order α_s^2 terms in both the matching functions and the RG exponents. For the matching functions H_{ui} and \tilde{j} this counting is unambiguous: they are both needed at two loops. The H_{ui} to this order can be derived from the calculations in [20–23], and \tilde{j} was calculated to NNLO in [24]; for the convenience of the reader, we list the results in the Appendix. As for the RG exponents, to define their NNLO expansion requires assumptions about the matching scales μ_h, μ_i , and μ_0 . By default, we shall assume the hierarchy $\mu_h \gg \mu_i \gg \mu_0$. In that case, to account for all of the α_s^2 pieces in the RG exponents requires Γ_{cusp} to four loops and the anomalous dimensions a_{γ^J} and $a_{\gamma'}$ to three loops. However, both γ' and Γ_{cusp} are known to one loop lower, which adds a small uncertainty to the analysis. For the missing pieces, we shall use the [1,1] Padé approximation described in the Appendix. In practice, we shall always use $\mu_0 = 1.5 \text{ GeV}$ in next section, so that $\mu_i \sim \mu_0$. In that case the general expression (13) resums some higher-order logarithms which are not large.

To evaluate the partial decay rates requires a model for the shape function $\hat{S}(\hat{\omega}, \mu_0)$. Experimental information on the shape function is provided by data on the photon energy spectrum in $\bar{B} \rightarrow X_s \gamma$ decays, and can be used to guide the functional form of the model. In addition, model-independent constraints are provided by the fact that moments of the shape function, defined as [7, 8]

$$M_N(\hat{\omega}_0, \mu) = \int_0^{\hat{\omega}_0} d\hat{\omega} \hat{\omega}^N \hat{S}(\hat{\omega}, \mu), \tag{14}$$

can be calculated in a local heavy-quark expansion, as long as $\hat{\omega}_0 \gg \Lambda_{\text{QCD}}$ [7, 25]. In the renormalization scheme referred to as the shape-function scheme [7, 25], the shape-function

moments are used to define the heavy-quark parameters order-by-order in perturbation theory. Limiting ourselves to the first two moments, which is sufficient to order $1/m_b^2$ in the heavy-quark expansion, one has

$$\begin{aligned}\frac{M_1(\mu_f + \bar{\Lambda}(\mu_f, \mu), \mu)}{M_0(\mu_f + \bar{\Lambda}(\mu_f, \mu), \mu)} &= \bar{\Lambda}(\mu_f, \mu), \\ \frac{M_2(\mu_f + \bar{\Lambda}(\mu_f, \mu), \mu)}{M_0(\mu_f + \bar{\Lambda}(\mu_f, \mu), \mu)} &= \frac{\mu_\pi^2(\mu_f, \mu)}{3} + \bar{\Lambda}^2(\mu_f, \mu),\end{aligned}\tag{15}$$

where $\bar{\Lambda} = M_B - m_b$ and μ_π^2 is related to the kinetic-energy parameter in HQET. Requiring that a given shape-function model correctly reproduces the moment relations (15) puts constraints on its parameters. These constraints depend on the order in perturbation theory at which the moments are evaluated. In the numerical analysis, we shall always use the constraints obtained from the two-loop moments. The moments to this order can be calculated as explained in [25], using the two-loop expression for the quantity $s(L, \mu)$ obtained in [26]. In addition to the perturbative expressions, one needs numerical values for $\bar{\Lambda}(\mu_f, \mu)$ and $\mu_\pi^2(\mu_f, \mu)$. These can be determined from global fits for the HQET parameters in other renormalization schemes using perturbative conversion relations. For the choice of scales $\mu_f = \mu = \mu_*$, the connection with the pole scheme reads [25]

$$\begin{aligned}m_b^{\text{pole}} &= m_b(\mu_*, \mu_*) + \mu_* \frac{4\alpha_s(\mu_*)}{3\pi} \left[1 + \frac{\alpha_s(\mu_*)}{\pi} \left(\frac{271}{36} + \frac{7\pi^2}{36} - \frac{17}{12} \zeta_3 - \frac{47}{54} n_f \right) \right] \\ &\quad + \frac{\mu_\pi^2(\mu_*, \mu_*)}{\mu_*} \left(\frac{\alpha_s(\mu_*)}{\pi} \right)^2 \left(-\frac{13}{81} + \frac{17}{27} \zeta_3 + \frac{10}{243} n_f \right), \\ -\lambda_1^{\text{pole}} &= \mu_\pi^2(\mu_*, \mu_*) \left[1 - \frac{2\alpha_s(\mu_*)}{3\pi} + \left(\frac{\alpha_s(\mu_*)}{\pi} \right)^2 \left(\frac{19}{18} - \frac{7\pi^2}{54} - \frac{17}{6} \zeta_3 - \frac{n_f}{9} \right) \right] \\ &\quad + \mu_*^2 \left(\frac{\alpha_s(\mu_*)}{\pi} \right)^2 \left(-\frac{20}{9} + \frac{17}{6} \zeta_3 + \frac{14}{27} n_f \right).\end{aligned}\tag{16}$$

In the rest of the paper, we will use the notation $m_b(\mu_*, \mu_*) \equiv m_b^*$ and $\mu_\pi^2(\mu_*, \mu_*) \equiv \mu_\pi^{*2}$ for the HQET parameters in the shape-function scheme, evaluated at the scale $\mu_* = 1.5$ GeV. Recent HFAG numbers for these parameters are $m_b^* = (4.707_{-0.053}^{+0.059})$ GeV and $\mu_\pi^{*2} = (0.216_{-0.076}^{+0.054})$ GeV² [1]. They are determined from information on $\bar{B} \rightarrow X_c l \bar{\nu}_l$ moments alone, under the assumption that moments from $B \rightarrow X_s \gamma$ decays should not be used in the global fits, on grounds that the measurements are typically made at values of the photon energy where shape-function effects are expected to be non-negligible [3]. To obtain numerical values for the non-diagonal parameters $m_b(\mu_f, \mu)$ and $\mu_\pi^2(\mu_f, \mu)$, one uses the generalization of (16) given in [25], along with the fact that the pole scheme parameters are scale independent.

In the analysis that follows, we model the shape function as

$$\hat{S}(\hat{\omega}, \mu_0) = \mathcal{N}(b, \Lambda) \hat{\omega}^{b-1} \exp\left(-\frac{b\hat{\omega}}{\Lambda}\right).\tag{17}$$

The normalization factor \mathcal{N} , as well as the model parameters b and Λ , are tuned to satisfy the two-loop moment constraints described above. To get a feeling for how this compares

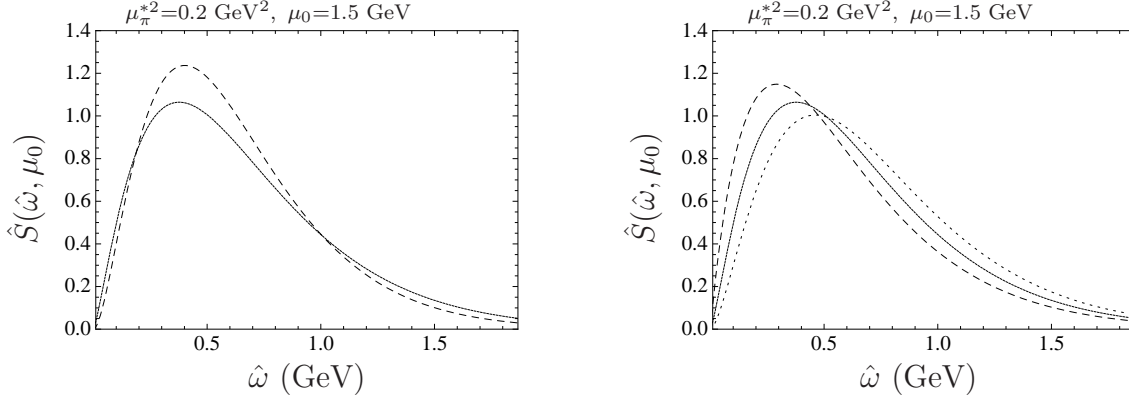


Figure 1: Left: model of the shape-function with the moment relations evaluated at one-loop order (dashed) and two-loop order (solid), for $m_b^* = 4.71$ GeV. Right: model of the shape-function with the moment relations evaluated at two loops, for $m_b^* = 4.66$ GeV (dotted), $m_b^* = 4.71$ GeV (solid), and $m_b^* = 4.77$ GeV (dashed).

with the model generated from the one-loop moments and used in [8], we show in the left-hand plot of Figure 1 the shape-function model (17) tuned to reproduce the moment relations for $m_b^* = 4.71$ GeV and $\mu_\pi^{*2} = 0.2$ GeV² at one- and two-loop order. In both cases, we use the four-loop running coupling with $\alpha_s(M_z) = 0.1176$, and match onto the four-flavor theory at 4.25 GeV. The results also depend on the UV cutoff of the moment integration range, which we choose as $\hat{\omega}_0 = M_B - 2E_0$, with $E_0 = 1.8$ GeV. We furthermore take $\mu_0 = 1.5$ GeV. The figure shows that the shape-function model generated using the two-loop moment relations has a smaller average value for $\hat{\omega} < 1.0$ GeV compared to that generated with the one-loop moments. Since to leading order in α_s a given partial rate is directly proportional to the integral of the shape function over a window specified by the cut, the model with the two-loop constraints tends to yield lower values for partial decay rates with kinematics restricted to the shape-function region. In the right-hand plot of Figure 1 we show the shape-function model generated using the NNLO moment relations for three different values of m_b^* , which cover the range of the HFAG values quoted above. The models with higher m_b^* have a noticeably larger average value for $\hat{\omega} \lesssim 0.5$ GeV, but the difference starts to become smaller for values of $\hat{\omega}$ higher than this. This implies that raising m_b^* tends to raise partial decay rates in the shape-function region, and that this effect is largest for the most restrictive cuts. We shall see in the next section that the changes in the shape-function model for different values of m_b^* constitute the largest parametric uncertainty in the $|V_{ub}|$ analysis.

Since the emphasis of this paper is the study of the perturbative series for a given shape function model, in the numerical studies we limit ourselves to the shape-function model (17), with the moment constraints implemented as explained above. Recently, a different procedure for building shape-function models which satisfy the moment constraints was proposed in [27]. It would be interesting to see to what extent the numerical results change when using such models at common values of the HQET parameters and the scale μ_0 , but we do not explore this issue in the current work.

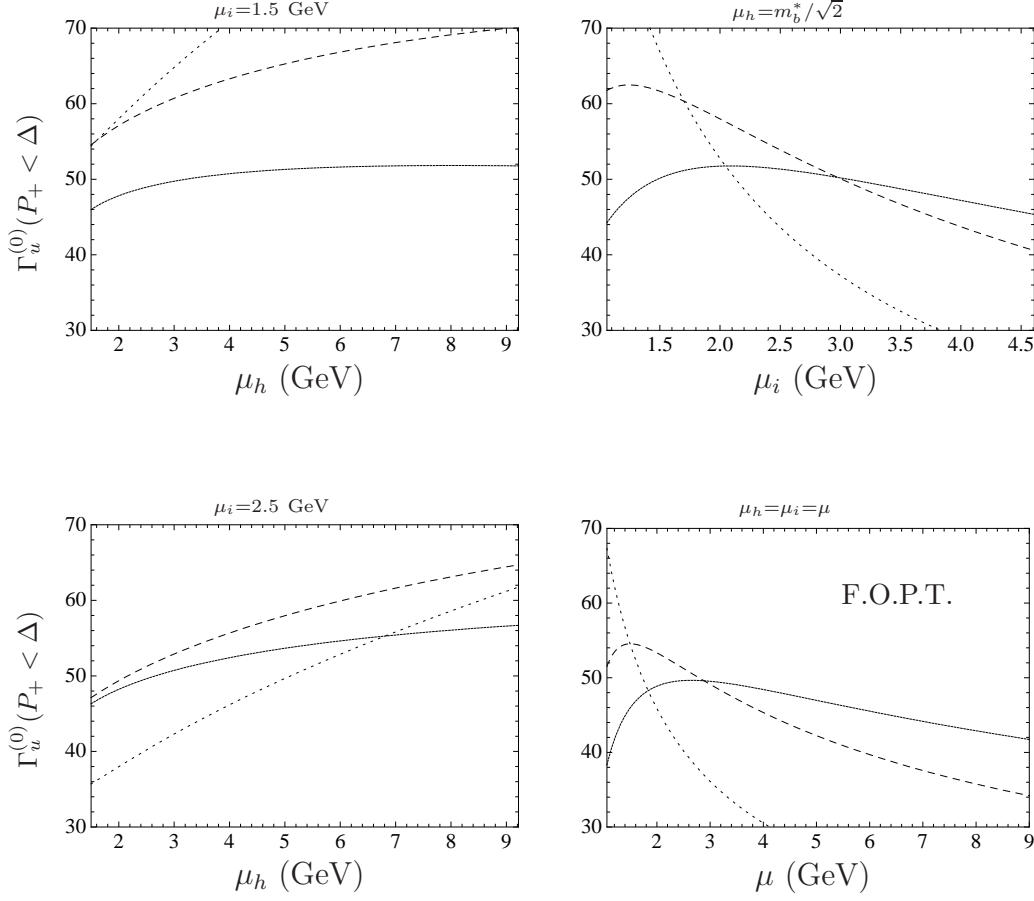


Figure 2: Dependence of the partial rate $\Gamma_u^{(0)}$ (in units of $|V_{ub}|^2 \text{ ps}^{-1}$) with a cut on $P_+ < \Delta = 0.66 \text{ GeV}$ on the matching scales μ_h and μ_i at LO (dotted), NLO (dashed), and NNLO (solid), with the parameter choices $m_b^* = 4.71 \text{ GeV}$ and $\mu_\pi^{*2} = 0.2 \text{ GeV}^2$. The case $\mu_h = \mu_i = \mu$ corresponds to fixed-order perturbation theory (F.O.P.T.).

3 Numerical results for leading-power partial rates

In this section we study the effects of the NNLO perturbative corrections to the leading-power term $\Gamma_u^{(0)}$. For the time being, we limit ourselves to three benchmark partial rates, defined by the following cuts:

1. $P_+ < 0.66 \text{ GeV}$
2. $M_X < 1.7 \text{ GeV}$
3. $E_l > 2.0 \text{ GeV}$

Experimental data is available for each of these partial decay rates, and will be used to extract values of $|V_{ub}|$ in the next section. The goal of this section is to address the following questions:

- How does the NNLO analysis change the central values and error estimates compared to NLO?
- Is resummation important, or is fixed-order perturbation theory sufficient?

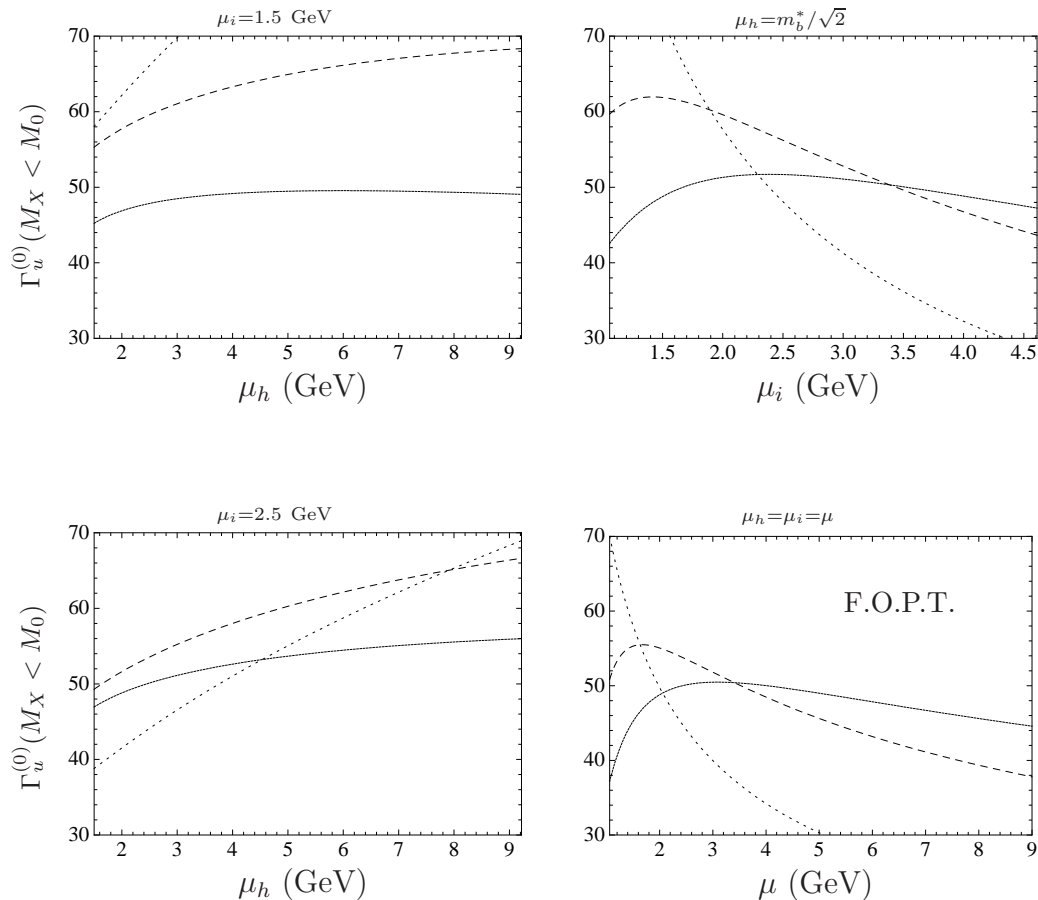


Figure 3: Dependence of the partial rate $\Gamma_u^{(0)}$ (in units of $|V_{ub}|^2 \text{ ps}^{-1}$) with a cut on $M_X < M_0 = 1.7 \text{ GeV}$ on the matching scales μ_h and μ_i at LO (dotted), NLO (dashed), and NNLO (solid), with the parameter choices $m_b^* = 4.71 \text{ GeV}$ and $\mu_\pi^{*2} = 0.2 \text{ GeV}^2$. The case $\mu_h = \mu_i = \mu$ corresponds to fixed-order perturbation theory.

- How well do the NNLO corrections in the large- β_0 limit approximate the full results?

We shall examine these issues in the following subsections, with the help of the information contained in Figures 2-7, and the numbers given in Section 3.3. Before interpreting the results, we first make some comments on the numerical evaluations. To study the behavior of the perturbative expansion, we give results where the structure functions (13) are evaluated at LO, NLO, and NNLO. In doing this, we evaluate the product of matching functions $H \cdot \tilde{j}$ and the RG-exponents $S, \eta, a_{\gamma^J}, a_{\gamma'}$ to the given order in α_s . These quantities also depend on the renormalization scheme for m_b , which we choose as the shape-function scheme; the shifts from the pole scheme are made using the perturbative relations (16) as appropriate at a given order in α_s . At this point we evaluate the resulting expressions numerically, without any further expansion. This means, for example, that we do not use relations such as $y^{a_{\Gamma, \text{LO}} + b\alpha_s} \approx y^{a_{\Gamma, \text{LO}}} (1 + b\alpha_s \ln y)$ (we have checked that the difference between the two expansions is negligible numerically). Finally, we use a common shape function when quoting results at LO, NLO, and NNLO, namely that where the moment constraints are implemented at NNLO. For reference, at $m_b^* = 4.71 \text{ GeV}$ and $\mu_\pi^{*2} = 0.2 \text{ GeV}^2$, the shape-function model is $\hat{S}(\hat{\omega}) = 2.78 \text{ GeV}^{-1} \Omega^{1.29} \exp(-\Omega)$, where $\Omega = \hat{\omega} \times 3.42 \text{ GeV}^{-1}$.

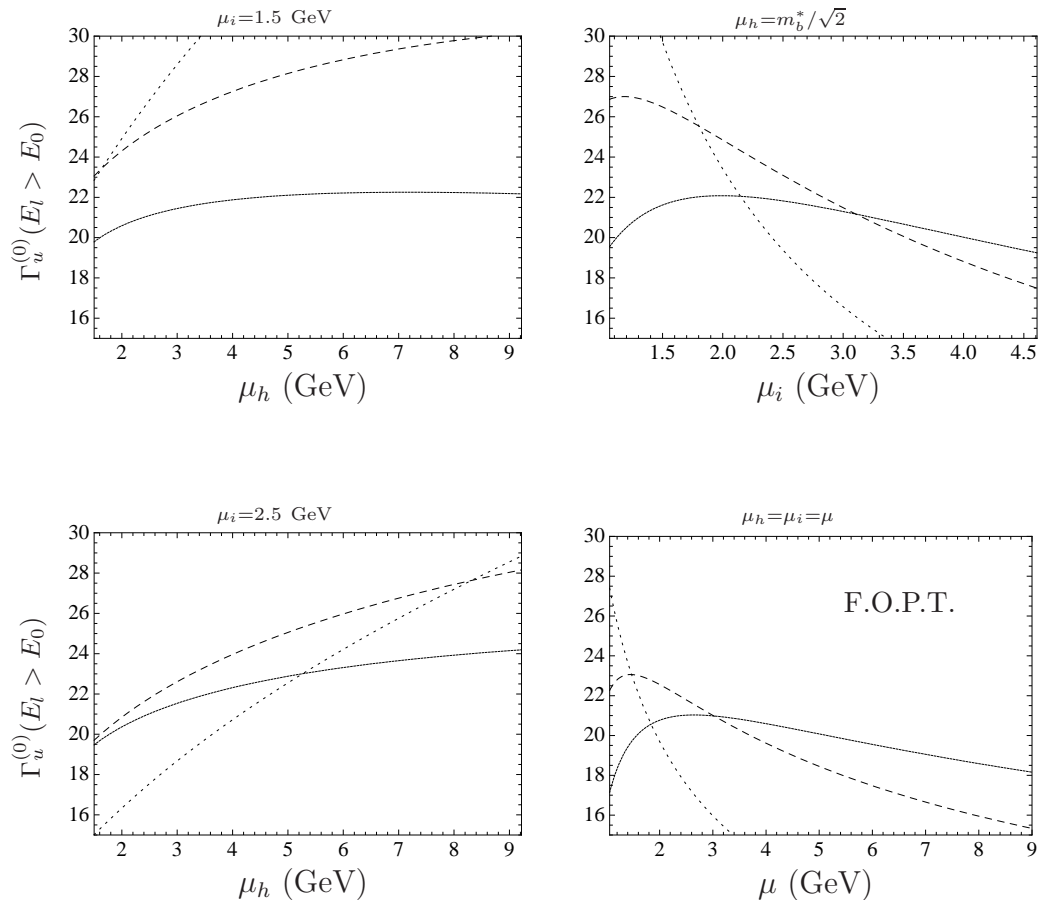


Figure 4: Dependence of the partial rate $\Gamma_u^{(0)}$ (in units of $|V_{ub}|^2 \text{ ps}^{-1}$) with a cut on $E_l > E_0 = 2.0 \text{ GeV}$ on the matching scales μ_h and μ_i at LO (dotted), NLO (dashed), and NNLO (solid), with the parameter choices $m_b^* = 4.71 \text{ GeV}$ and $\mu_\pi^{*2} = 0.2 \text{ GeV}^2$. The case $\mu_h = \mu_i = \mu$ corresponds to fixed-order perturbation theory.

A further issue is the treatment of the charm-quark mass. The dependence on this parameter first enters at NNLO, through diagrams where a charm loop is inserted into a gluon propagator. In evaluating the perturbative expressions, we always set $n_h = 1$ and work with $n_l = 4$ light flavors. In other words, we treat $m_c \ll \mu_i$ and set $m_c = 0$ when the fermion loops needed for the calculation of the two-loop hard and jet functions contain a charm quark. The calculations from [23] show that this is not a bad approximation to the full dependence in the hard function H . Numerically, it may be more appropriate to treat $m_c \sim \mu_i$, as discussed in the context of SCET in [28, 29], but a consistent treatment would also require the m_c dependence in the jet function, which is not yet available.

A final complication is that the analytic expression for the hard function H_{u1} contains a harmonic polylogarithm (HPL) of weight four, which cannot be expressed in terms of standard functions such as polylogarithms and their generalizations. For the numerical evaluation of HPLs we have used the **Mathematica** package HPL [30], and the **FORTRAN** subroutine **hplog** [31].

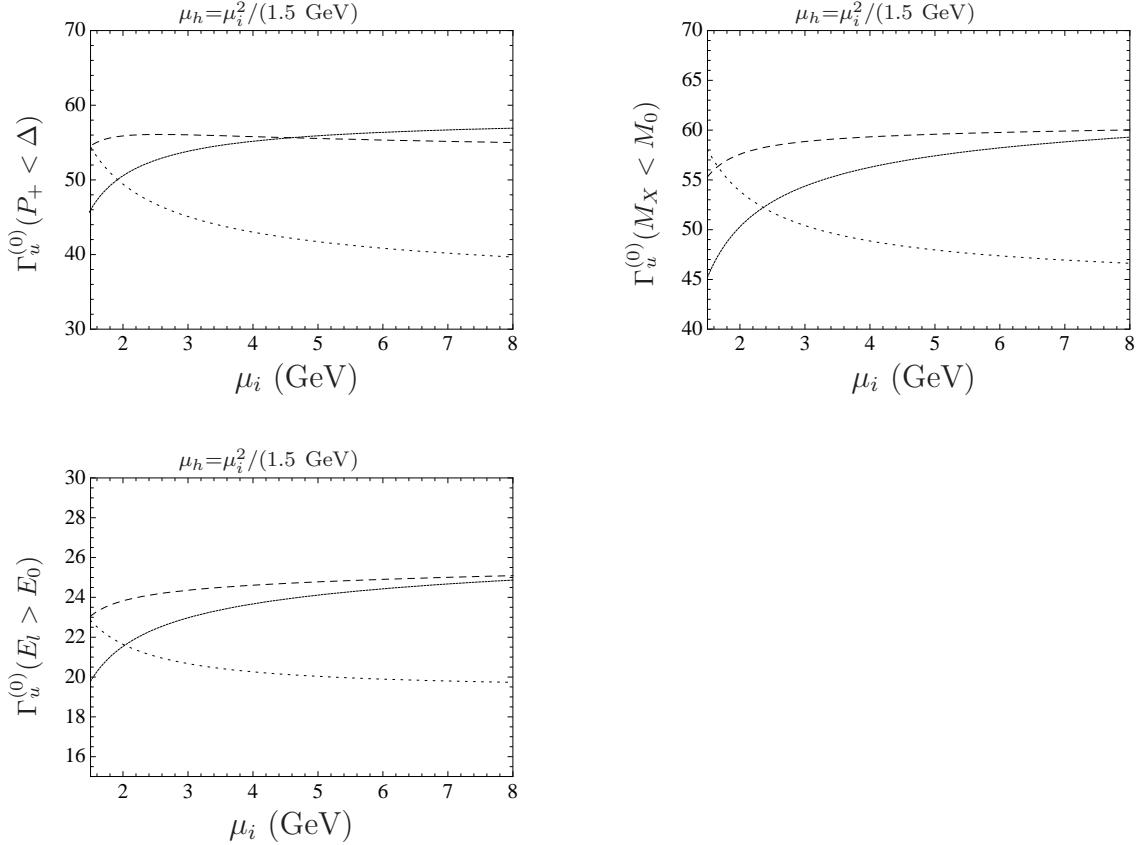


Figure 5: Dependence of partial rates (in units of $|V_{ub}|^2 \text{ps}^{-1}$) on μ_i , with $\mu_h = \mu_i^2/(1.5 \text{ GeV})$, at LO (dotted), NLO (dashed), and NNLO (solid), for the cuts $P_+ < \Delta = 0.66 \text{ GeV}$, $M_X < M_0 = 1.7 \text{ GeV}$, and $E_l > E_0 = 2.0 \text{ GeV}$. In each case $\mu_\pi^{*2} = 0.2 \text{ GeV}^2$.

3.1 Impact of NNLO corrections on central values and errors

The first question we wish to address is how the NNLO corrections and implementation of the dependence on the scale μ_i affect the central values and error estimates for the leading-power partial decay rates compared to the NLO analysis in [8]. We have shown in Figures 2-4 a set of plots meant to shed light on that issue. To compare central values obtained at different orders in perturbation theory we have shown in the upper-left hand plots of Figures 2-4 the dependence on the scale μ_h , for the fixed value $\mu_i = 1.5 \text{ GeV}$, which is the BLNP choice. We see that for this choice of μ_i the NNLO corrections are quite large in each case, and significantly lower the central values compared to NLO. At the same time, the perturbative uncertainties associated with the matching scale μ_h are reduced, as indicated by the flattening of the curves at higher orders in perturbation theory.

A new element of our analysis compared to the procedure in [8] is that the matching scale μ_i is not necessarily fixed to the value $\mu_i = 1.5 \text{ GeV}$. In the upper right-hand plots of Figures 2-4, we display the dependence of the results on the scale μ_i , for fixed values $\mu_h = m_b^*/\sqrt{2}$. We note a large dependence on the intermediate scale at NLO, which is reduced but still significant at NNLO. Because the dependence on μ_i is so strong at NLO, even small changes of the value of μ_i can alter rather drastically the agreement between the NLO and NNLO results. To illustrate this effect we have shown in the bottom

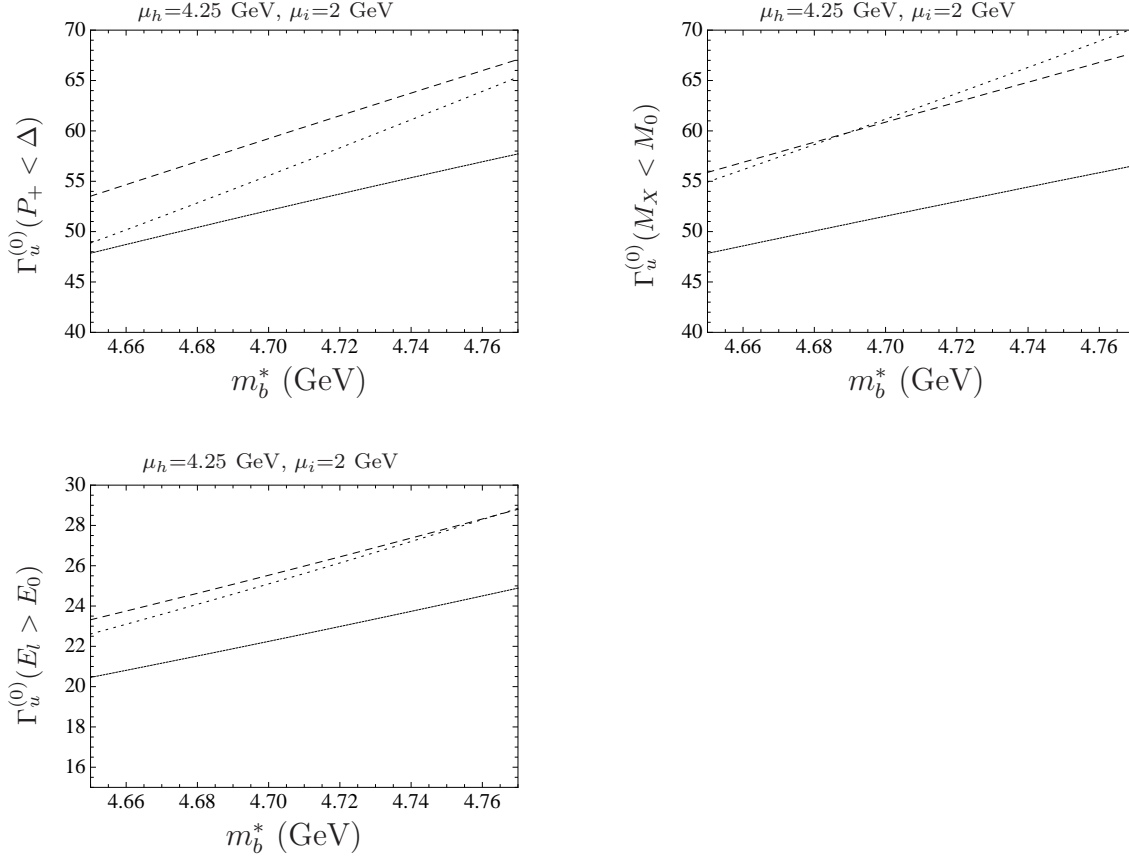


Figure 6: Dependence of partial rates (in units of $|V_{ub}|^2 \text{ ps}^{-1}$) on m_b^* at LO (dotted), NLO (dashed), and NNLO (solid), for the cuts $P_+ < \Delta = 0.66 \text{ GeV}$, $M_X < M_0 = 1.7 \text{ GeV}$, and $E_l > E_0 = 2.0 \text{ GeV}$. In each case $\mu_\pi^{*2} = 0.2 \text{ GeV}^2$.

left-hand plots of Figures 2-4 the dependence of the partial rates on μ_h for $\mu_i = 2.5 \text{ GeV}$, which is higher than the BLNP choice. This higher value of the intermediate scale brings the NLO results into closer agreement with the NNLO results.

So far, we have fixed one of the two matching scales to a default value and studied the behavior of the partial decay rates under variations of the other. Another option is to establish a correlation between the scales and vary them simultaneously. Setting them equal to one another corresponds to fixed-order perturbation theory and will be discussed in the next section. A different choice, which is somewhat more natural in SCET, is to vary the scales such that the relation $\mu_h \sim \mu_i^2/\mu_s$ is respected, where μ_s is a typical soft scale. In Figure 5, we show the behavior of the partial rates under such a correlated variation for the choice $\mu_s = 1.5 \text{ GeV}$. It is remarkable that the NLO result is almost entirely stable under scale variations. This feature appears to be accidental, since at NNLO the scale dependence actually becomes stronger under this correlated running.

In addition to the unphysical dependence on the matching scales μ_h and μ_i , the partial rates contain a rather strong parametric dependence on the numerical value of the b -quark mass m_b^* , mainly through the moment constraints on the shape-function model; scaling relations for this dependence were derived in [8]. We have already shown in Figure 1 how changing m_b^* distorts the shape-function model. We show in Figure 6 how these changes in the model translate into changes in the partial rates in the range $4.65 \text{ GeV} < m_b^* < 4.77 \text{ GeV}$. Obviously, the present uncertainty in the value of the b -quark

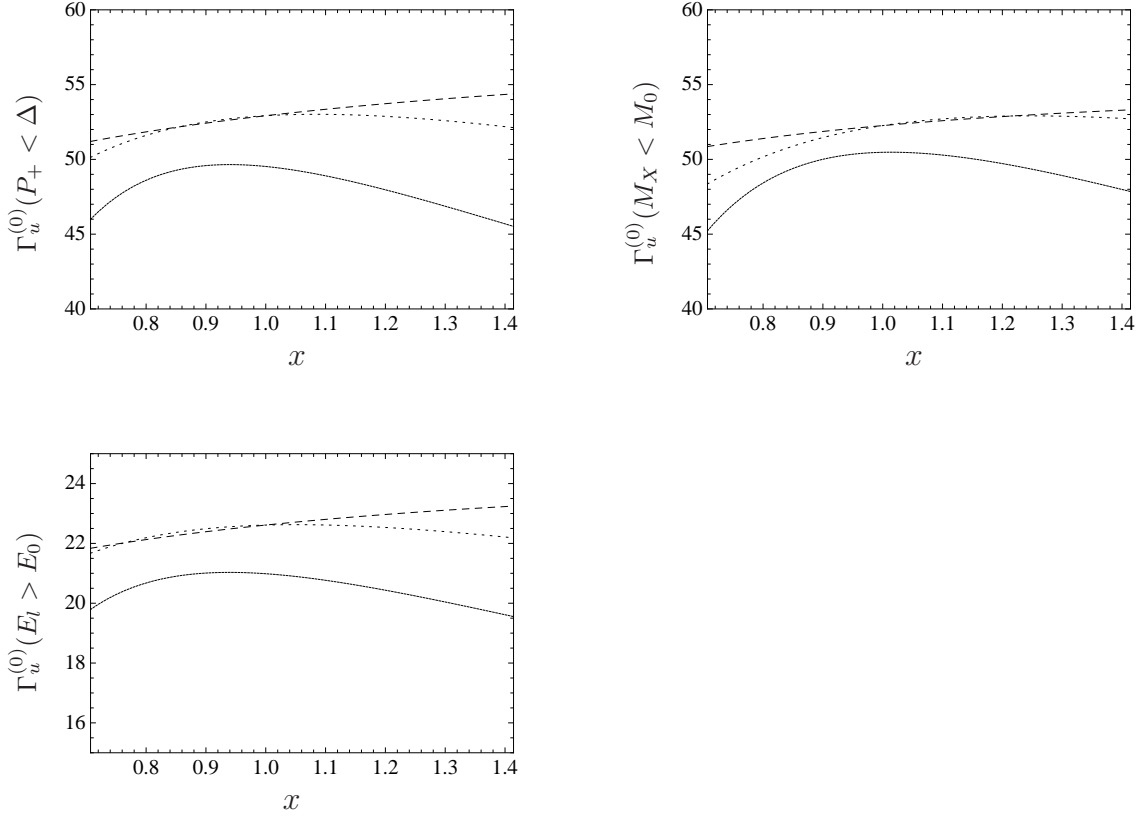


Figure 7: Comparison of the NNLO partial rates $\Gamma_u^{(0)}$ (in units of $|V_{ub}|^2 \text{ ps}^{-1}$) in resummed perturbation theory and fixed order, for the cuts $P_+ < \Delta = 0.66 \text{ GeV}$, $M_X < M_0 = 1.7 \text{ GeV}$, and $E_l > E_0 = 2.0 \text{ GeV}$. The dashed line is the variation of the resummed results with $\mu_h = (4.25 \text{ GeV})x$, for $\mu_i = 2 \text{ GeV}$, the dotted line is the variation with $\mu_i = (2 \text{ GeV})x$, for $\mu_h = 4.25 \text{ GeV}$, and the solid line is the variation of the fixed order result with $\mu = (3 \text{ GeV})x^2$. In all cases $m_b^* = 4.71 \text{ GeV}$ and $\mu_\pi^{*2} = 0.2 \text{ GeV}^2$.

mass adds a large parametric uncertainty to the analysis.

From the above discussion we can conclude that, compared to BLNP analysis in [8], where $\mu_i = 1.5 \text{ GeV}$, the net effect of the NNLO corrections is to lower the central values for partial rates by around 15–20%, while at the same time reducing the perturbative uncertainty on the scale μ_h . Moreover, we have pointed out that there is a considerable dependence on the scale μ_i at NLO, which is reduced but still significant even at NNLO. To make these statements more quantitative, we give central values and error estimates for some input parameters. In particular, we choose the values $\mu_i^{\text{def}} = 2.0 \text{ GeV}$ and $\mu_h^{\text{def}} = 4.25 \text{ GeV}$, and then vary the scales in the range $1/\sqrt{2} < \mu_{h,i}/\mu_{h,i}^{\text{def}} < \sqrt{2}$. We then find for the three benchmark partial rates, in units of $|V_{ub}|^2 \text{ ps}^{-1}$:

- $P_+ < 0.66 \text{ GeV}$:

	$\Gamma_u^{(0)}$	μ_h	μ_i
NLO	60.37	+3.52 −3.37	+3.81 −6.67
NNLO	52.92	+1.46 −1.72	+0.09 −2.79

- $M_X < 1.7$ GeV:

	$\Gamma_u^{(0)}$	μ_h	μ_i
NLO	61.86	+3.23 -3.21	+1.89 -5.50
NNLO	52.26	+1.05 -1.40	+0.65 -3.90

- $E_l > 2.0$ GeV:

	$\Gamma_u^{(0)}$	μ_h	μ_i
NLO	25.98	+1.63 -1.61	+1.69 -2.81
NNLO	22.61	+0.63 -0.78	+0.01 -0.94

The default numbers refer to the value of the partial rate for $\mu_{h,i} = \mu_{h,i}^{\text{def}}$. To obtain the uncertainties associated with variations of μ_h , we keep μ_i fixed to its default value, and then assign upper (lower) errors by picking out the highest (lowest) value of the decay rate in the range $1/\sqrt{2} < \mu_h/\mu_h^{\text{def}} < \sqrt{2}$; the procedure for μ_i is analogous.

3.2 Comparison with fixed-order perturbation theory

In this section we compare the results from RG-improved perturbation theory with those obtained in a fixed-order calculation. The standard argument to motivate the use of resummed perturbation theory is that even though logs of μ_h/μ_i are not particularly large, the running coupling constant runs quickly at low scales $\mu_i \sim 1.5$ GeV, so the scale separation between the hard and jet scales is important. If this were the case, we would expect to see a large scale dependence in the fixed-order result. To test whether this actually happens, we have shown in the bottom right plots of Figures 2-4 the results where the matching scales are set to $\mu_h = \mu_i = \mu$, which corresponds to fixed-order perturbation theory. We see that the NNLO results are rather stable under variations of μ from 1.5 GeV to $2m_b^*$. Also, the convergence of the perturbation series is actually better than in resummed perturbation theory, in the sense that the NNLO results lie within the ranges covered by varying the renormalization scale μ in the LO and NLO results.

To illustrate further the differences between resummed and fixed-order perturbation theory we show in Figure 7 the NNLO results for both cases. After the substitutions indicated in the caption, the curves can be used to compare the fixed-order results in the range $\mu = (1.5 - 6)$ GeV with the resummed results in the ranges $1/\sqrt{2} < \mu_{h,i}/\mu_{h,i}^{\text{def}} < \sqrt{2}$, with $\mu_i^{\text{def}} = 2.0$ GeV and $\mu_h^{\text{def}} = 4.25$ GeV. In this way, the scale in the fixed-order result is varied in a range which very nearly covers the lowest value of μ_i to the highest value of μ_h . To compare results more closely, we list tables of central values and errors, to be compared with the resummed results in the previous section. We choose the default scale as $\mu = 3.0$ GeV, and quote the uncertainty obtained by varying it up and down by a factor of two. We then find, in units of $|V_{ub}|^2 \text{ ps}^{-1}$:

- $P_+ < 0.66$ GeV:

Fixed-Order	$\Gamma_u^{(0)}$	μ
NLO	49.11	+5.43 -9.41
NNLO	49.53	+0.13 -4.01

- $M_X < 1.7$ GeV:

Fixed-Order	$\Gamma_u^{(0)}$	μ
NLO	51.81	+3.69 -8.62
NNLO	50.47	+0.01 -2.62

- $E_l > 2.0$ GeV:

Fixed-Order	$\Gamma_u^{(0)}$	μ
NLO	21.01	+2.04 -3.54
NNLO	20.99	+0.04 -1.43

At NNLO the errors are comparable with the resummed results from the previous section. In each case the central values for the fixed-order results are noticeably lower than the resummed ones.

The analysis above indicates that, for the leading-order term in the SCET expansion, the factorization of the perturbative coefficient multiplying the leading-order shape function into jet and hard functions is not strictly necessary: using the fixed-order results does not lead to large scale uncertainties compared to the treatment in RG-improved perturbation theory, nor to a poor convergence of the perturbative expansion. Given this fact, it is legitimate to ask whether “kinematic” power corrections, namely those suppressed by the perturbative ratio of jet to hard scales and scaling as $P_+/P_- \sim \Lambda_{\text{QCD}}/m_b$ in the shape-function region, should be treated separately from the leading-order term. The one-loop analysis in [8] shows that the $1/m_b$ expansion of these kinematic power corrections converges very quickly, and that the leading-order term is indeed of the size expected of a $1/m_b$ correction. To check this at two loops would require the calculation of the hadronic tensor in fixed-order perturbation theory to this order, which has yet to be done. While partial results in the large- β_0 limit are available, we shall see in the next section that, for the leading-order term, they do not accurately approximate the full two-loop calculations. In absence of evidence to the contrary, we shall assume that ignoring the kinematically suppressed two-loop corrections provides an accurate approximation of decay rates to this order.

3.3 NNLO corrections in the large- β_0 limit

We now give illustrative results for the case where the large- β_0 approximation to the two-loop hard and jet functions is used. To obtain these results, we pick out the $n_l C_F$ color structure in the α_s^2 corrections to $H \cdot \tilde{j}$, and then set $n_l \rightarrow -3\beta_0/2$. As a check on our results, we have confirmed that convoluting the resulting expression with the large- β_0 limit of the partonic shape function evaluated at NNLO in [26], and setting all matching scales to a common scale μ , we reproduce the NNLO corrections to the partial rate with a cut on P_+ obtained in the large- β_0 limit in [32] (these can also be obtained from the triple differential result in [33]). To compare numerical values of partial decay rates in the large- β_0 limit with the exact ones, we evaluate the hard and jet functions at a common scale $\mu_h = \mu_i = 1.5$ GeV. Furthermore, we choose $m_b^* = 4.71$ GeV and $\mu_\pi^{*2} = 0.2$ GeV²,

and convolute both results with a common shape function obtained by implementing the moment constraints at NNLO. Then the full NNLO results for $\Gamma_u^{(0)}$, labeled “QCD”, and the large- β_0 results, labeled “BLM”, read for the three cuts (in units of $|V_{ub}| \text{ ps}^{-1}$):

- $P_+ < 0.66 \text{ GeV}$:

$$\text{QCD: } 54.43 + 0.11 [\alpha_s] + (-3.68 [h] - 0.26 [j] - 4.61 [h j] = -8.55) [\alpha_s^2] = 45.99$$

$$\text{BLM: } 54.43 + 0.11 [\alpha_s] + (-14.1 [h] + 14.1 [j] = -0.02) [\alpha_s^2] = 54.52$$

- $M_X < 1.7 \text{ GeV}$:

$$\text{QCD: } 58.06 - 2.76 [\alpha_s] + (-4.05 [h] - 1.99 [j] - 4.04 [h j] = -10.1) [\alpha_s^2] = 45.22$$

$$\text{BLM: } 58.06 - 2.76 [\alpha_s] + (-15.7 [h] + 13.0 [j] = -2.68) [\alpha_s^2] = 52.62$$

- $E_l > 2.0 \text{ GeV}$:

$$\text{QCD: } 22.85 + 0.21 [\alpha_s] + (-1.64 [h] + 0.65 [j] - 2.28 [h j] = -3.27) [\alpha_s^2] = 19.79$$

$$\text{BLM: } 22.85 + 0.21 [\alpha_s] + (-7.12 [h] + 6.32 [j] = -0.80) [\alpha_s^2] = 22.26$$

We have included labels to distinguish the contributions from different orders in α_s , and for the NNLO pieces we have also indicated whether the contribution comes from the hard function ($[h]$), the jet function ($[j]$), or the product of one-loop hard and jet functions ($[h j]$). We see that the contributions of the two-loop hard and jet functions in the large- β_0 approximation are larger than the full results. In each case, they undergo large cancellations in the sum and give results which are much smaller in magnitude than the complete ones. Given the poor agreement of results in the large- β_0 approximation with the full NNLO results for the leading order term in the HQET expansion, it is somewhat questionable that including only such terms leads to any phenomenological improvement compared to NLO. For the jet function \tilde{j} , the poor agreement between the full results and those in the large- β_0 limit was previously noted in [24].

4 Impact on the extraction of $|V_{ub}|$

In this section we study the numerical impact of our results on the extraction of $|V_{ub}|$ from experimental information on partial decay rates. In order to do so, we combine our NNLO results for the leading-power term $\Gamma_u^{(0)}$ with the power corrections obtained in [8]. A given partial rate Γ_u is then obtained in the form

$$\Gamma_u = \Gamma_u^{(0)} + [(\Gamma_u^{\text{kin}(1)} + \Gamma_u^{\text{had}(1)}) + (\Gamma_u^{\text{kin}(2)} + \Gamma_u^{\text{had}(2)})]_{\text{BLNP}}. \quad (18)$$

The power corrections from the BLNP analysis are split into hadronic contributions, involving subleading shape functions [34–36], and kinematic contributions, which account for terms suppressed by powers of $P_+/M_B \sim P_+/P_-$ and thus scaling as Λ_{QCD}/M_B in the shape-function region¹. The hadronic terms are treated at tree level, and the kinematic terms at one loop.

¹For a recent analysis of these corrections in terms of subleading jet functions in SCET, see [37].

We summarize our results in the tables of numbers below, for the three partial rates studied in the previous section, as well as for different values of the E_l and M_X cuts. The central values and errors are obtained as follows. First, we evaluate the leading-power term $\Gamma_u^{(0)}$ as in Section 3.1. We choose the default scales as $\mu_h^{\text{def}} = 4.25$ GeV and $\mu_i^{\text{def}} = 2.0$ GeV, and the HQET parameters as $m_b^* = 4.707$ GeV and $\mu_\pi^{*2} = 0.216$ GeV². Then, we evaluate the power-suppressed terms *exactly* as in [8], for the same choice of HQET parameters as for the leading term. Adding these two numbers together gives a default value for Γ_u . To this default value we assign uncertainties coming from a number of different sources. To associate uncertainties with the HQET parameters, we vary them simultaneously in the leading-order term and power corrections, and assign errors for the ranges $m_b^* = (4.707^{+0.059}_{-0.053})$ GeV and $\mu_\pi^{*2} = (0.216^{+0.054}_{-0.076})$ GeV². To estimate perturbative uncertainties associated with the choice of matching scales in the leading term, we vary the default choices for μ_h and μ_i up and down by a factor of $\sqrt{2}$, and add these in quadrature to obtain the uncertainty labeled $\mu_{h,i}$ in the tables. Perturbative scales also appear in the power corrections, through resummation factors, and through the scale $\bar{\mu}$ for the kinematic power corrections. We vary these as in [8], and add the different sources of perturbative uncertainty in quadrature to obtain the total perturbative uncertainty for the power corrections, labeled μ_{pow} in the tables. Finally, we associate errors with the functional variation of the subleading shape functions, called SSF in the tables, and add an uncertainty of $\delta\Gamma_u^{\text{WA}} = \pm 1.26|V_{ub}|^2\text{ps}^{-1}$ to take account weak annihilation effects (not shown in the table). The analysis shows that the uncertainty from m_b^* is the dominant one. To quote the uncertainties in such a way that isolates this effect, we add all of the others in quadrature to obtain a total uncertainty *excluding* that associated with m_b^* , which we instead quote in the last column of the tables. The results read (in units of $|V_{ub}|^2\text{ps}^{-1}$):

- $P_+ < 0.66$ GeV:

	Γ_u	$\mu_{h,i}$	μ_{pow}	μ_π^{*2}	SSF	tot	m_b^*
NLO	54.28	+5.07 -7.36	+1.91 -1.48	+1.27 -1.07	± 1.41	+5.87 -7.81	+8.20 -7.05
NNLO	46.77	+1.44 -3.29	+1.91 -1.48	+2.08 -1.56	± 1.41	+3.69 -4.36	+6.34 -5.48

- $M_X < 1.55$ GeV:

	Γ_u	$\mu_{h,i}$	μ_{pow}	μ_π^{*2}	SSF	tot	m_b^*
NLO	54.73	+4.68 -7.08	+1.99 -1.31	+1.02 -0.94	± 1.30	+5.50 -7.48	+8.02 -6.87
NNLO	47.09	+1.22 -3.44	+1.99 -1.31	+1.79 -1.42	± 1.30	+3.46 -4.34	+6.26 -5.41

- $M_X < 1.7$ GeV:

	Γ_u	$\mu_{h,i}$	μ_{pow}	μ_π^{*2}	SSF	tot	m_b^*
NLO	61.21	+3.69 -6.29	+2.48 -1.60	+1.85 -1.46	± 0.63	+5.02 -6.80	+7.36 -6.42
NNLO	51.60	+1.24 -4.13	+2.48 -1.60	+2.28 -1.72	± 0.63	+3.85 -4.95	+5.80 -5.05

Method	$\Delta\mathcal{B}^{\text{exp}} [10^{-4}]$	$ V_{ub} [10^{-3}]$ NLO	$ V_{ub} [10^{-3}]$ NNLO
$E_l > 2.1 \text{ GeV}$ CLEO [38]	$3.3 \pm 0.2 \pm 0.7$	$3.56 \pm 0.40^{+0.48+0.31}_{-0.27-0.26}$	$3.81 \pm 0.43^{+0.33+0.31}_{-0.21-0.26}$
$E_l > 2.0 \text{ GeV}$ BABAR [39]	$5.7 \pm 0.4 \pm 0.5$	$3.97 \pm 0.22^{+0.37+0.26}_{-0.23-0.25}$	$4.30 \pm 0.24^{+0.26+0.28}_{-0.20-0.27}$
$E_l > 1.9 \text{ GeV}$ BELLE [40]	$8.5 \pm 0.4 \pm 1.5$	$4.27 \pm 0.39^{+0.32+0.25}_{-0.19-0.22}$	$4.65 \pm 0.43^{+0.27+0.27}_{-0.18-0.24}$
$M_X < 1.7 \text{ GeV}$ BELLE [41]	$12.3 \pm 1.1 \pm 1.2$	$3.55 \pm 0.24^{+0.22+0.21}_{-0.13-0.19}$	$3.87 \pm 0.26^{+0.21+0.21}_{-0.13-0.19}$
$M_X < 1.55 \text{ GeV}$ BABAR [42]	$11.7 \pm 0.9 \pm 0.7$	$3.67 \pm 0.18^{+0.29+0.26}_{-0.17-0.24}$	$3.96 \pm 0.19^{+0.20+0.26}_{-0.13-0.24}$
$P_+ < 0.66 \text{ GeV}$ BELLE [41]	$11.0 \pm 1.0 \pm 1.6$	$3.56 \pm 0.31^{+0.30+0.27}_{-0.17-0.23}$	$3.84 \pm 0.33^{+0.21+0.26}_{-0.13-0.22}$
$P_+ < 0.66 \text{ GeV}$ BABAR [42]	$9.4 \pm 1.0 \pm 0.8$	$3.30 \pm 0.23^{+0.27+0.25}_{-0.16-0.22}$	$3.55 \pm 0.24^{+0.19+0.24}_{-0.13-0.21}$

Table 1: Values of $|V_{ub}|$ determined at NLO and NNLO, for the parameter values discussed in the text. The uncertainties in the experimental measurements of $\Delta\mathcal{B}^{\text{exp}}$ are statistical and systematic, respectively. In the columns labeled $|V_{ub}|$ the first error is experimental, the second is the sum of all theoretical and parametric errors *except* for that from m_b^* , and the third is that from m_b^* . We have combined errors of the same type by adding in quadrature, and used $\tau_B = 1.584 \text{ ps}$ for the average B -meson lifetime.

- $E_l > 1.9 \text{ GeV}$:

	Γ_u	$\mu_{h,i}$	μ_{pow}	μ_{π}^{*2}	SSF	tot	m_b^*
NLO	29.21	$+2.14$ -3.29	$+1.52$ -1.01	$+0.63$ -0.51	± 0.53	$+3.03$ -3.73	$+3.51$ -2.91
NNLO	24.65	$+0.63$ -1.61	$+1.52$ -1.01	$+0.75$ -0.60	± 0.53	$+2.27$ -2.41	$+2.95$ -2.43

- $E_l > 2.0 \text{ GeV}$:

	Γ_u	$\mu_{h,i}$	μ_{pow}	μ_{π}^{*2}	SSF	tot	m_b^*
NLO	22.76	$+2.34$ -3.23	$+1.19$ -0.88	$+0.44$ -0.35	± 0.59	$+3.00$ -3.64	$+3.23$ -2.66
NNLO	19.38	$+0.63$ -1.22	$+1.19$ -0.88	$+0.60$ -0.46	± 0.59	$+2.03$ -2.10	$+2.70$ -2.21

- $E_l > 2.1 \text{ GeV}$:

	Γ_u	$\mu_{h,i}$	μ_{pow}	μ_{π}^{*2}	SSF	tot	m_b^*
NLO	16.30	$+2.50$ -3.05	$+0.97$ -0.89	$+0.19$ -0.16	± 0.70	$+3.05$ -3.49	$+2.87$ -2.31
NNLO	14.17	$+0.64$ -1.06	$+0.97$ -0.89	$+0.38$ -0.29	± 0.70	$+1.89$ -2.02	$+2.39$ -1.93

From these numbers and the corresponding experimental results, we arrive at the values of $|V_{ub}|$ listed in Table 1. An examination of the table shows that the NNLO corrections shift the values of $|V_{ub}|$ upwards by roughly 10% compared to NLO.

5 Conclusions

We studied the impact of NNLO perturbative corrections on the leading term in the $1/m_b$ expansion for partial decay rates in $\bar{B} \rightarrow X_u l \bar{\nu}_l$ decays. These corrections were implemented within a modified form of the BLNP framework, which allows for variations of both the perturbative jet scale μ_i and the hard-matching scale μ_h in the resummed partial rates. The particular choice $\mu_i = \mu_h$ corresponds to fixed-order perturbation theory, which allowed us to perform a detailed comparison between fixed-order results and the resummed results from BLNP. Within resummed perturbation theory, we found that the dependence on the intermediate scale μ_i introduces sizeable perturbative uncertainties at NLO, which are reduced but still significant at NNLO. For the conventional choice $\mu_i = 1.5$ GeV used in previous analyses in the BLNP formalism, the NNLO corrections also induce fairly large downward shifts in the partial rates. For higher values of μ_i and in fixed-order perturbation theory, these shifts are more moderate. We also compared between the full NNLO results in fixed-order perturbation theory and those obtained in the large- β_0 approximation. We found that the large- β_0 approximation for the NNLO corrections provides a poor approximation to the full results, at least for the leading-order term in the $1/m_b$ expansion. Whether this would also be true upon the inclusion of terms suppressed by kinematic factors of P_+/M_B , which are small in the shape-function region, is an open question. Finally, we combined our new results for the leading-order partial rates with the known power corrections up to $1/m_b^2$, and showed how our analysis impacts the determination of $|V_{ub}|$ from several experimental measurements. For parameter and scale choices typically used in current analyses within the BLNP framework, the effect of the NNLO corrections is to raise the value of $|V_{ub}|$ by slightly less than 10% compared to NLO; the exact results are shown in Table 1.

Acknowledgments: C.G. is partially supported by the Swiss National Foundation as well as EC-Contract MRTN-CT-2006-035482 (FLAVIANet). The Albert Einstein Center for Fundamental Physics (Bern) is supported by the “Innovations- und Kooperationsprojekt C-13 of the Schweizerische Universitätskonferenz SUK/CRUS”.

A Appendix

A.1 The hard and jet functions

The hard functions H_{ui} are derived from the SCET Wilson coefficients C_i , which arise when matching the QCD $b \rightarrow u$ transition current onto SCET. The two-loop QCD calculations needed for the NNLO analysis were recently completed in [20–23]. In terms of the quantities $H_{ij} = C_i C_j$, the H_{ui} read

$$H_{u1} = H_{11}, \quad H_{u2} = 0, \quad H_{u3} = \frac{2H_{13} + H_{33}}{y} + H_{12} + H_{23} + \frac{y}{4}H_{22}. \quad (\text{A1})$$

The Laplace transformed jet function \tilde{j} was calculated to NNLO in [24]. To two-loop order, the result is

$$\tilde{j}(L, \mu) = 1 + \frac{C_F \alpha_s}{4\pi} \left(2L^2 - 3L + 7 - \frac{2\pi^2}{3} \right) + C_F \left(\frac{\alpha_s}{4\pi} \right)^2 [C_F J_F + C_A J_A + T_F n_f J_f], \quad (\text{A2})$$

where

$$\begin{aligned} J_F &= 2L^4 - 6L^3 + \left(\frac{37}{2} - \frac{4\pi^2}{3} \right) L^2 + \left(-\frac{45}{2} + 4\pi^2 - 24\zeta_3 \right) L + \frac{205}{8} - \frac{97\pi^2}{12} + \frac{61\pi^4}{90} - 6\zeta_3, \\ J_A &= -\frac{22}{9} L^3 + \left(\frac{367}{18} - \frac{2\pi^2}{3} \right) L^2 + \left(-\frac{3155}{54} + \frac{11\pi^2}{9} + 40\zeta_3 \right) L \\ &\quad + \frac{53129}{648} - \frac{155\pi^2}{36} - \frac{37\pi^4}{180} - 18\zeta_3, \\ J_f &= \frac{8}{9} L^3 - \frac{58}{9} L^2 + \left(\frac{494}{27} - \frac{4\pi^2}{9} \right) L - \frac{4057}{162} + \frac{13\pi^2}{9}. \end{aligned} \quad (\text{A3})$$

A.2 Renormalization-group factors and anomalous dimensions

Here we list the perturbative expansion of the renormalization-group functions in (10) up to NNLO. To do this, we first define the expansion coefficients of the cusp anomalous dimension and QCD β -function as

$$\begin{aligned} \Gamma_{\text{cusp}}(\alpha_s) &= \Gamma_0 \frac{\alpha_s}{4\pi} + \Gamma_1 \left(\frac{\alpha_s}{4\pi} \right)^2 + \Gamma_2 \left(\frac{\alpha_s}{4\pi} \right)^3 + \Gamma_3 \left(\frac{\alpha_s}{4\pi} \right)^4 + \dots, \\ \beta(\alpha_s) &= -2\alpha_s \left[\beta_0 \frac{\alpha_s}{4\pi} + \beta_1 \left(\frac{\alpha_s}{4\pi} \right)^2 + \beta_2 \left(\frac{\alpha_s}{4\pi} \right)^3 + \beta_3 \left(\frac{\alpha_s}{4\pi} \right)^4 + \dots \right], \end{aligned} \quad (\text{A4})$$

and similarly for the other anomalous dimensions. In terms of these quantities, the function a_Γ is given by [17, 19]

$$\begin{aligned} a_\Gamma(\nu, \mu) &= \frac{\Gamma_0}{2\beta_0} \left\{ \ln \frac{\alpha_s(\mu)}{\alpha_s(\nu)} + \left(\frac{\Gamma_1}{\Gamma_0} - \frac{\beta_1}{\beta_0} \right) \frac{\alpha_s(\mu) - \alpha_s(\nu)}{4\pi} \right. \\ &\quad \left. + \left[\frac{\Gamma_2}{\Gamma_0} - \frac{\beta_2}{\beta_0} - \frac{\beta_1}{\beta_0} \left(\frac{\Gamma_1}{\Gamma_0} - \frac{\beta_1}{\beta_0} \right) \right] \frac{\alpha_s^2(\mu) - \alpha_s^2(\nu)}{32\pi^2} + \dots \right\}. \end{aligned} \quad (\text{A5})$$

Note that this result involves the three-loop anomalous dimension, which is known for the cusp anomalous dimension and for a_{γ^J} , but not for the anomalous dimension $a_{\gamma'}$. The result for the Sudakov factor S is [19]

$$\begin{aligned}
S(\nu, \mu) = & \frac{\Gamma_0}{4\beta_0^2} \left\{ \frac{4\pi}{\alpha_s(\nu)} \left(1 - \frac{1}{r} - \ln r \right) + \left(\frac{\Gamma_1}{\Gamma_0} - \frac{\beta_1}{\beta_0} \right) (1 - r + \ln r) + \frac{\beta_1}{2\beta_0} \ln^2 r \right. \\
& + \frac{\alpha_s(\nu)}{4\pi} \left[\left(\frac{\beta_1\Gamma_1}{\beta_0\Gamma_0} - \frac{\beta_2}{\beta_0} \right) (1 - r + r \ln r) + \left(\frac{\beta_1^2}{\beta_0^2} - \frac{\beta_2}{\beta_0} \right) (1 - r) \ln r \right. \\
& \quad \left. \left. - \left(\frac{\beta_1^2}{\beta_0^2} - \frac{\beta_2}{\beta_0} - \frac{\beta_1\Gamma_1}{\beta_0\Gamma_0} + \frac{\Gamma_2}{\Gamma_0} \right) \frac{(1-r)^2}{2} \right] \right. \\
& + \left(\frac{\alpha_s(\nu)}{4\pi} \right)^2 \left[\left(\frac{\beta_1\beta_2}{\beta_0^2} - \frac{\beta_1^3}{2\beta_0^3} - \frac{\beta_3}{2\beta_0} + \frac{\beta_1}{\beta_0} \left(\frac{\Gamma_2}{\Gamma_0} - \frac{\beta_2}{\beta_0} + \frac{\beta_1^2}{\beta_0^2} - \frac{\beta_1\Gamma_1}{\beta_0\Gamma_0} \right) \frac{r^2}{2} \right) \ln r \right. \\
& \quad + \left(\frac{\Gamma_3}{\Gamma_0} - \frac{\beta_3}{\beta_0} + \frac{2\beta_1\beta_2}{\beta_0^2} + \frac{\beta_1^2}{\beta_0^2} \left(\frac{\Gamma_1}{\Gamma_0} - \frac{\beta_1}{\beta_0} \right) - \frac{\beta_2\Gamma_1}{\beta_0\Gamma_0} - \frac{\beta_1\Gamma_2}{\beta_0\Gamma_0} \right) \frac{(1-r)^3}{3} \\
& \quad + \left(\frac{3\beta_3}{4\beta_0} - \frac{\Gamma_3}{2\Gamma_0} + \frac{\beta_1^3}{\beta_0^3} - \frac{3\beta_1^2\Gamma_1}{4\beta_0^2\Gamma_0} + \frac{\beta_2\Gamma_1}{\beta_0\Gamma_0} + \frac{\beta_1\Gamma_2}{4\beta_0\Gamma_0} - \frac{7\beta_1\beta_2}{4\beta_0^2} \right) (1-r)^2 \\
& \quad \left. \left. + \left(\frac{\beta_1\beta_2}{\beta_0^2} - \frac{\beta_3}{\beta_0} - \frac{\beta_1^2\Gamma_1}{\beta_0^2\Gamma_0} + \frac{\beta_1\Gamma_2}{\beta_0\Gamma_0} \right) \frac{1-r}{2} \right] + \dots \right\}, \tag{A6}
\end{aligned}$$

where $r = \alpha_s(\mu)/\alpha_s(\nu)$. Whereas the three-loop anomalous dimensions and β -function are required in (A5), the expression for S also involves the four-loop coefficients Γ_3 and β_3 .

We now list expressions for the anomalous dimensions and the QCD β -function, quoting all results in the $\overline{\text{MS}}$ renormalization scheme. The expansion of the cusp anomalous dimension Γ_{cusp} to two-loop order was obtained some time ago [43], while recently the three-loop coefficient has been obtained in [44]. For the four-loop coefficient Γ_3 , we follow [45] and use its [1,1] Padé approximant, $\Gamma_3 \approx \Gamma_2^2/\Gamma_1$. The results are

$$\begin{aligned}
\Gamma_0 &= 4C_F, \\
\Gamma_1 &= 4C_F \left[\left(\frac{67}{9} - \frac{\pi^2}{3} \right) C_A - \frac{20}{9} T_F n_f \right], \\
\Gamma_2 &= 4C_F \left[C_A^2 \left(\frac{245}{6} - \frac{134\pi^2}{27} + \frac{11\pi^4}{45} + \frac{22}{3} \zeta_3 \right) + C_A T_F n_f \left(-\frac{418}{27} + \frac{40\pi^2}{27} - \frac{56}{3} \zeta_3 \right) \right. \\
&\quad \left. + C_F T_F n_f \left(-\frac{55}{3} + 16\zeta_3 \right) - \frac{16}{27} T_F^2 n_f^2 \right], \\
\Gamma_3 &\approx 7849, 4313, 1553 \quad \text{for } n_f = 3, 4, 5. \tag{A7}
\end{aligned}$$

The SCET anomalous dimension γ' was deduced at two loops using RG-invariance along with results for the jet and shape function anomalous dimensions in [17], and was

confirmed through the explicit calculations in [20–23]. The result is

$$\begin{aligned}\gamma'_0 &= -5C_F, \\ \gamma'_1 &= -8C_F \left[\left(\frac{3}{16} - \frac{\pi^2}{4} + 3\zeta_3 \right) C_F + \left(\frac{1549}{432} + \frac{7\pi^2}{48} - \frac{11}{4}\zeta_3 \right) C_A - \left(\frac{125}{216} + \frac{\pi^2}{24} \right) n_f \right].\end{aligned}\tag{A8}$$

To evaluate the RG-factor $a_{\gamma'}$ at NNLO requires the three-loop anomalous dimension, which is not yet known. For that, we use the [1,1] Padé approximation, $\gamma'_2 \approx \gamma'^2_1/\gamma'_0$. Although this same approximation works well for Γ_{cusp} it works poorly for γ_J , as can be verified using the explicit results listed in [19]:

$$\begin{aligned}\gamma^J_0 &= -3C_F, \\ \gamma^J_1 &= C_F^2 \left(-\frac{3}{2} + 2\pi^2 - 24\zeta_3 \right) + C_F C_A \left(-\frac{1769}{54} - \frac{11\pi^2}{9} + 40\zeta_3 \right) + C_F T_F n_f \left(\frac{242}{27} + \frac{4\pi^2}{9} \right) \\ \gamma^J_2 &= C_F^3 \left(-\frac{29}{2} - 3\pi^2 - \frac{8\pi^4}{5} - 68\zeta_3 + \frac{16\pi^2}{3}\zeta_3 + 240\zeta_5 \right) \\ &\quad + C_F^2 C_A \left(-\frac{151}{4} + \frac{205\pi^2}{9} + \frac{247\pi^4}{135} - \frac{844}{3}\zeta_3 - \frac{8\pi^2}{3}\zeta_3 - 120\zeta_5 \right) \\ &\quad + C_F C_A^2 \left(-\frac{412907}{2916} - \frac{419\pi^2}{243} - \frac{19\pi^4}{10} + \frac{5500}{9}\zeta_3 - \frac{88\pi^2}{9}\zeta_3 - 232\zeta_5 \right) \\ &\quad + C_F^2 T_F n_f \left(\frac{4664}{27} - \frac{32\pi^2}{9} - \frac{164\pi^4}{135} + \frac{208}{9}\zeta_3 \right) \\ &\quad + C_F C_A T_F n_f \left(-\frac{5476}{729} + \frac{1180\pi^2}{243} + \frac{46\pi^4}{45} - \frac{2656}{27}\zeta_3 \right) \\ &\quad + C_F T_F^2 n_f^2 \left(\frac{13828}{729} - \frac{80\pi^2}{81} - \frac{256}{27}\zeta_3 \right).\end{aligned}\tag{A9}$$

Finally, the expansion coefficients for the QCD β -function to four-loop order are

$$\begin{aligned}\beta_0 &= \frac{11}{3} C_A - \frac{4}{3} T_F n_f, \\ \beta_1 &= \frac{34}{3} C_A^2 - \frac{20}{3} C_A T_F n_f - 4C_F T_F n_f, \\ \beta_2 &= \frac{2857}{54} C_A^3 + \left(2C_F^2 - \frac{205}{9} C_F C_A - \frac{1415}{27} C_A^2 \right) T_F n_f + \left(\frac{44}{9} C_F + \frac{158}{27} C_A \right) T_F^2 n_f^2 \\ \beta_3 &= \frac{149753}{6} + 3564\zeta_3 - \left(\frac{1078361}{162} + \frac{6508}{27}\zeta_3 \right) n_f + \left(\frac{50065}{162} + \frac{6472}{81}\zeta_3 \right) n_f^2 + \frac{1093}{729} n_f^3,\end{aligned}\tag{A10}$$

where β_3 is taken from [46] and is evaluated for $N_c = 3$.

References

- [1] E. Barberio *et al.* [Heavy Flavor Averaging Group], arXiv:0808.1297 [hep-ex].
- [2] M. Antonelli *et al.*, arXiv:0907.5386 [hep-ph].
- [3] M. Neubert, arXiv:0801.0675 [hep-ph].
- [4] M. Neubert, Phys. Rev. D **49**, 3392 (1994) [arXiv:hep-ph/9311325].
- [5] M. Neubert, Phys. Rev. D **49**, 4623 (1994) [arXiv:hep-ph/9312311].
- [6] I. I. Y. Bigi, M. A. Shifman, N. G. Uraltsev and A. I. Vainshtein, Int. J. Mod. Phys. A **9**, 2467 (1994) [arXiv:hep-ph/9312359].
- [7] S. W. Bosch, B. O. Lange, M. Neubert and G. Paz, Nucl. Phys. B **699** (2004) 335 [arXiv:hep-ph/0402094].
- [8] B. O. Lange, M. Neubert and G. Paz, Phys. Rev. D **72** (2005) 073006 [arXiv:hep-ph/0504071].
- [9] P. Gambino, P. Giordano, G. Ossola and N. Uraltsev, JHEP **0710** (2007) 058 [arXiv:0707.2493 [hep-ph]].
- [10] J. R. Andersen and E. Gardi, JHEP **0601** (2006) 097 [arXiv:hep-ph/0509360].
- [11] C. W. Bauer, S. Fleming, D. Pirjol and I. W. Stewart, Phys. Rev. D **63**, 114020 (2001) [arXiv:hep-ph/0011336].
- [12] C. W. Bauer, D. Pirjol and I. W. Stewart, Phys. Rev. D **65** (2002) 054022 [arXiv:hep-ph/0109045].
- [13] M. Beneke, A. P. Chapovsky, M. Diehl and T. Feldmann, Nucl. Phys. B **643**, 431 (2002) [arXiv:hep-ph/0206152].
- [14] G. P. Korchemsky and G. Sterman, Phys. Lett. B **340**, 96 (1994) [arXiv:hep-ph/9407344].
- [15] R. Akhouri and I. Z. Rothstein, Phys. Rev. D **54** (1996) 2349 [arXiv:hep-ph/9512303].
- [16] C. W. Bauer and A. V. Manohar, Phys. Rev. D **70** (2004) 034024 [arXiv:hep-ph/0312109].
- [17] M. Neubert, Eur. Phys. J. C **40**, 165 (2005) [arXiv:hep-ph/0408179].
- [18] T. Becher and M. Neubert, Phys. Rev. Lett. **97** (2006) 082001 [arXiv:hep-ph/0605050].
- [19] T. Becher, M. Neubert and B. D. Pecjak, JHEP **0701** (2007) 076 [arXiv:hep-ph/0607228].
- [20] R. Bonciani and A. Ferroglia, JHEP **0811** (2008) 065 [arXiv:0809.4687 [hep-ph]].

- [21] H. M. Asatrian, C. Greub and B. D. Pecjak, Phys. Rev. D **78**, 114028 (2008) [arXiv:0810.0987 [hep-ph]].
- [22] M. Beneke, T. Huber and X. Q. Li, Nucl. Phys. B **811**, 77 (2009) [arXiv:0810.1230 [hep-ph]].
- [23] G. Bell, Nucl. Phys. B **812**, 264 (2009) [arXiv:0810.5695 [hep-ph]].
- [24] T. Becher and M. Neubert, Phys. Lett. B **637**, 251 (2006) [arXiv:hep-ph/0603140].
- [25] M. Neubert, Phys. Lett. B **612**, 13 (2005) [arXiv:hep-ph/0412241].
- [26] T. Becher and M. Neubert, Phys. Lett. B **633**, 739 (2006) [arXiv:hep-ph/0512208].
- [27] Z. Ligeti, I. W. Stewart and F. J. Tackmann, Phys. Rev. D **78** (2008) 114014 [arXiv:0807.1926 [hep-ph]].
- [28] H. Boos, T. Feldmann, T. Mannel and B. D. Pecjak, Phys. Rev. D **73** (2006) 036003 [arXiv:hep-ph/0504005].
- [29] H. Boos, T. Feldmann, T. Mannel and B. D. Pecjak, JHEP **0605** (2006) 056 [arXiv:hep-ph/0512157].
- [30] D. Maitre, Comput. Phys. Commun. **174**, 222 (2006) [arXiv:hep-ph/0507152].
- [31] T. Gehrmann and E. Remiddi, Comput. Phys. Commun. **141** (2001) 296 [arXiv:hep-ph/0107173].
- [32] F. Campanario, M. Luke and S. Zuberi, arXiv:0811.1787 [hep-ph].
- [33] V. Aquila, P. Gambino, G. Ridolfi and N. Uraltsev, Nucl. Phys. B **719** (2005) 77 [arXiv:hep-ph/0503083].
- [34] K. S. M. Lee and I. W. Stewart, Nucl. Phys. B **721** (2005) 325 [arXiv:hep-ph/0409045].
- [35] S. W. Bosch, M. Neubert and G. Paz, JHEP **0411**, 073 (2004) [arXiv:hep-ph/0409115].
- [36] M. Beneke, F. Campanario, T. Mannel and B. D. Pecjak, JHEP **0506** (2005) 071 [arXiv:hep-ph/0411395].
- [37] G. Paz, JHEP **0906** (2009) 083 [arXiv:0903.3377 [hep-ph]].
- [38] A. Bornheim *et al.* [CLEO Collaboration], Phys. Rev. Lett. **88** (2002) 231803 [arXiv:hep-ex/0202019].
- [39] B. Aubert *et al.* [BABAR Collaboration], Phys. Rev. D **73**, 012006 (2006) [arXiv:hep-ex/0509040].
- [40] A. Limosani *et al.* [Belle Collaboration], Phys. Lett. B **621**, 28 (2005) [arXiv:hep-ex/0504046].

- [41] I. Bizjak *et al.* [Belle Collaboration], Phys. Rev. Lett. **95**, 241801 (2005) [arXiv:hep-ex/0505088].
- [42] B. Aubert *et al.* [BABAR Collaboration], Phys. Rev. Lett. **100**, 171802 (2008) [arXiv:0708.3702 [hep-ex]].
- [43] I. A. Korchemskaya and G. P. Korchemsky, Phys. Lett. B **287**, 169 (1992).
- [44] S. Moch, J. A. M. Vermaseren and A. Vogt, Nucl. Phys. B **688**, 101 (2004) [hep-ph/0403192].
- [45] S. Moch, J. A. M. Vermaseren and A. Vogt, Nucl. Phys. B **726**, 317 (2005) [hep-ph/0506288].
- [46] T. van Ritbergen, J. A. M. Vermaseren and S. A. Larin, Phys. Lett. B **400**, 379 (1997) [hep-ph/9701390].